Title: E Pluribus Unum: Functional Aggregation Enables Biological Ice Nucleation

Authors: Ralph Schwidetzky[1], Ingrid de Almeida Ribeiro[2], Nadine Bothen[3], Anna T. Backes[3], Arthur L. DeVries[4], Mischa Bonn[1], Janine Fröhlich-Nowoisky[3], Valeria Molinero[2], and Konrad Meister[1,5]

Affiliations:

[1]Max Planck Institute for Polymer Research, 55128 Mainz, Germany

[2]The University of Utah, 84112 Salt Lake City, UT, United States

[3]Max Planck Institute for Chemistry, 55128 Mainz, Germany

[4]University of Illinois at Urbana-Champaign, 61801 Urbana, IL, United States

[5]Boise State University, 83725 Boise, ID, United States

Classification:

Heterogeneous Ice Nucleation, Ice-Nucleating Proteins, Fungi, Protein Assembly

Abstract:

Biological ice nucleation plays a key role in the survival and adaptation of cold-adapted organisms. Several species of bacteria, fungi, and insects produce ice nucleators (INs) that enable ice formation of ice at temperatures above -10 ^{o}C. Bacteria and fungi produce particularly potent INs that can promote water crystallization above -5 ^{o}C. Bacterial INs consist of extended protein units that aggregate to achieve superior functionality. Despite decades of research, the nature and identity of fungal INs remain elusive. Here we combine ice-nucleation measurements, physicochemical characterization, numerical modeling and nucleation theory to shed light on the size and nature of the INs from the fungus *Fusarium acuminatum*. We find ice-binding and ice-shaping activity of *Fusarium* IN, suggesting a potential connection between ice growth promotion and inhibition. We demonstrate that fungal INs are composed of small 5.3 kDa protein subunits which assemble into ice-nucleating complexes that contain more than 100 subunits and have an ice-binding area of at least 250 nm^2. The potency of the INs is retained even when only the smaller subunits are initially present, suggesting robust pathways for their functional assembly in solution. We conclude that the use of small protein building blocks to build large IN assemblies is the common strategy among organisms to create potent biological INs.

Significance

Cold-blooded organisms have evolved efficient molecular strategies to control the nucleation and growth of ice. Although these strategies have developed independently across biological kingdoms, they all seem to rely on protein-building units to construct extended functional domains. Bacteria and insects use large proteinaceous units to obtain superior ice-nucleating complexes. However, the identity of fungal INs remains unknown. We show that small protein subunits, of which hundreds are capable of assembling in cell-free environments, make up fungal INs that enable ice formation at warm temperatures. Our findings highlight that nature has evolved a common *E pluribus unum* (out of many, one) strategy to enable high subzero ice nucleation temperatures by assembly of ice nucleating proteins into large functional aggregates.

The crystallization of water is the most prevalent liquid-to-solid phase transition on Earth. Ice formation is thermodynamically favored at temperatures below 0˚C, but the crystallization process is kinetically hindered by the cost of the ice nucleus interface. Consequently, pure water microdroplets can be supercooled to temperatures as low as −46 ˚C, below which homogenous ice nucleation seems to be unavoidable (1). In nature, the freezing of water is usually a heterogeneous process facilitated by ice nucleators (INs) of biological and abiotic origins. Natural occurring abiotic INs typically elevate freezing temperatures to −15 to −30 ˚C, whereas biological INs are more active and can facilitate freezing at temperatures between -2 and −15 ˚C (2). The benefits of ice nucleation for organisms from an ecological perspective, and its potential effects on cloud glaciation and precipitation are still not fully comprehended, and constitute a significant gap in our understanding of the relationship between climate and life.

The best-characterized biological INs are plant-associated bacteria of the genera *Pseudomonas*, *Pantoea*, and *Xanthomonas*, which enable ice formation at temperatures close to 0 ˚C (3). The ability of the ice-nucleating active bacteria to facilitate ice formation is attributed to ~120 kDa ice-nucleating proteins (INPs) that are anchored to their outer cell membrane, and that aggregate to achieve activity at high temperatures (4-6). The gene encoding the large INP units has been identified and found to be conserved across diverse ice-nucleating bacteria (7, 8). Besides bacteria, fungi produce very effective and the most widespread biological INs, enabling the crystallization of water at temperatures as warm as −2 ˚C (9, 10). The ice nucleation activity in fungi was first discovered in the genus *Fusarium*, and later observed in multiple other genera (e.g., *Isaria, Mortierella, Sarocladium, Puccinia*) (11-13). Ice-nucleating fungi can cause frost damage to plants, and have been found in rain, hail, and snow, suggesting that they may influence regional and global precipitation patterns (14-17). The cosmopolitan genus *Fusarium* comprises saprophytes and pathogens of plants and animals, and it is the most studied ice-nucleation-active fungus (9, 10). Although widely distributed in soil and on plants, it has also been detected in atmospheric and cloud water samples, making it a highly relevant biological and atmospheric model system (12, 18). The chemical composition and structures of the macromolecules responsible for ice nucleation activity in fungi remain unknown. Our current understanding suggests that *Fusarium* INs are cell-free secreted soluble macromolecules with a molecular weight lower than 100 kDa, and stable at pH values from 2 to 12 (9, 10, 19-21). The *Fusarium* INs were proposed to be at least partially proteinaceous, given their heat inactivation, peak UV absorbance at 280 nm, and sensitivity to certain proteinases (10, 21, 22). In addition, Vinatzer and coworkers recently identified over 200 candidates for ice-nucleation

genes, which code for secreted proteins at low temperatures, through comparative genomic and transcriptomics (21). Here, we investigate the composition, structure, and activity of INs from *Fusarium acuminatum,* which we purified from the surfaces of fungal spores and mycelia. We aim to identify the nature and size of the individual ice-nucleating macromolecules and estimate how many are involved in the aggregates responsible for these organisms' exceptional ice nucleation activity.

Results

To investigate the freezing capabilities of INs from spores and mycelial surfaces of *F. acuminatum*, aqueous *Fusarium* extracts were serially diluted tenfold, resulting in a concentration range spanning from ~14.1 mg/mL to ~1.41 ng/mL. For each concentration, the freezing of 96 3 µL-sized droplets was followed with a cooling rate of 1 ˚C/min (23). These measurements provide the fraction of frozen droplets as a function of temperature for each concentration. The results are combined using Vali's equation into a single freezing curve of *F. acuminatum*, shown in Fig. 1A, where N_m represents the total number of active INs above a certain temperature (24). The strong increase at −3.8 ˚C and the subsequent plateau in the cumulative number of INs per unit mass, $N_m(T)$ suggest the presence of a single population of highly efficient INs, consistent with previous studies (10, 21).

The high ice nucleation activity in *Fusarium* is indicative of INs capable of strong binding to ice (25). We employed ice affinity purification to capitalize on the ice-binding capabilities of the *Fusarium* INs to selectively purify them. The purification process involves the incorporation of the ice-binding INs into a slowly growing ice phase and the exclusion of non-ice-binding macromolecules and impurities (26, 27). Thereby, the ice-binding macromolecules present in *F. acuminatum* were isolated. The success of the process was assessed by monitoring the activity of the purified INs. The freezing curve of the ice-purified INs looks similar to that of the aqueous *Fusarium* extract, with a slight decrease in the total number of IN (Fig. 1A). The presence of ice-binding macromolecules in *Fusarium* was further investigated by measuring their ice-shaping capabilities. Using Nanoliter Cryoscopy we observed that when a ~15 µm ice disc was slowly cooled, faceting occurred, and the disc transformed into a hexagon, as shown in Fig. 1B. The presence of hexagonally shaped ice crystals confirms that the purified macromolecules in the *F. acuminatum* samples selectively bind to ice.

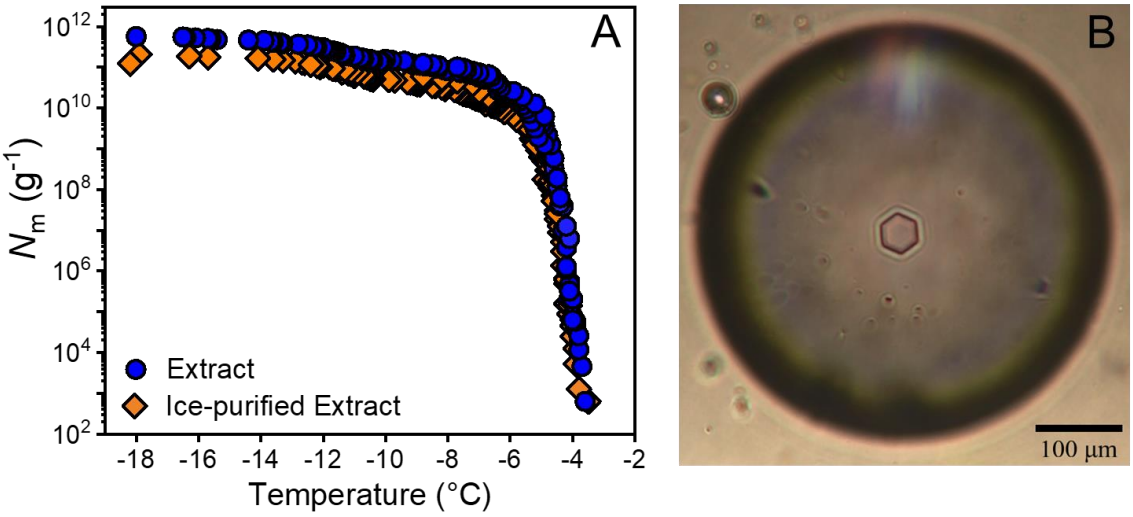

Fig. 1. Freezing experiments of aqueous extracts containing fungal ice nucleators from *F. acuminatum*. (A) Shown is the cumulative number of ice nucleators per unit mass of *F. acuminatum* (N_m) for extracts containing ice nucleators from spores and mycelial surfaces (blue) and for ice-purified ice nucleators (orange). (B) Cryomicroscopic image of a hexagonal ice crystal grown in a *F. acuminatum* IN extract.

The proteinaceous nature of the ice-binding macromolecules of *F. acuminatum* had been suggested, but was not previously confirmed (10). Fig. 2A shows circular dichroism (CD) spectra of the ice-purified solutions of *F. acuminatum* at room temperature and at 90 ºC. The CD spectrum of the untreated sample shows a maximum molar ellipticity at ~235 nm and a minimum at ~205 nm. Spectral analysis and fold recognition using BeStSel reveals that the *Fusarium* INs are proteinaceous with ~34% antiparallel β-sheet and ~18% helical content (28). In addition, the spectral shape shows similarities with CD spectra of assembled hydrophobins derived from the fungi *Grifola frondose (29).* It is further worth mentioning that high β-sheet contents were also found in ice-nucleating proteins (INPs) derived from bacteria (25, 27, 30). Upon heating the purified *Fusarium* INs, the CD spectrum shows marked changes: a reduction of the molar ellipticity at 235 nm, and a shift of the minimum at ~205 nm to ~202 nm. These spectral changes following heating to 90 °C suggest significant, irreversible changes in the secondary structure of the fungal INs. We interpret that these conformational changes cause an irreversible loss of the protein's native structure and are the origin of the observed elimination of *Fusarium*'s ice nucleation activity after heat treatment (Fig. 2B) (10).

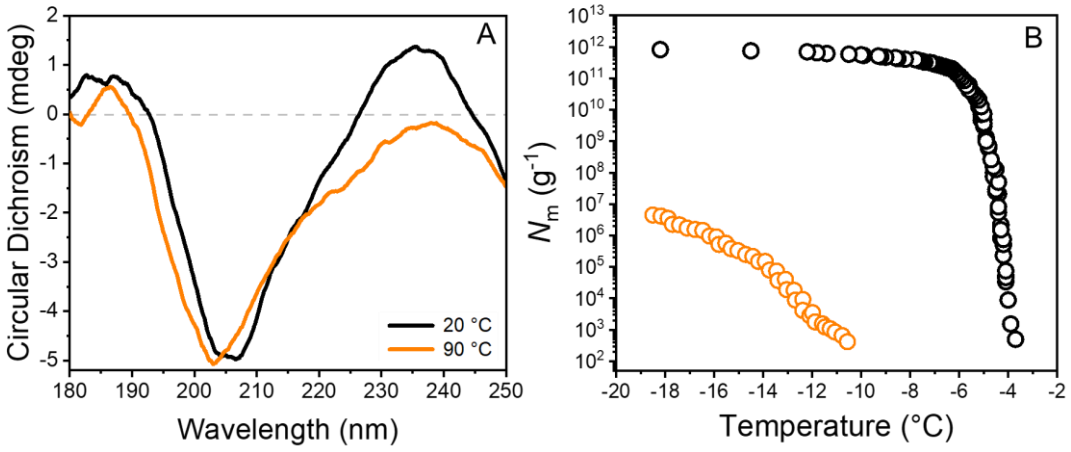

Fig. 2. Characterization of aqueous solutions containing ice-purified fungal INs from *F. acuminatum*. (A) The CD spectrum shows a maximum molar ellipticity at ~235 nm and a minimum at ~205 nm, and both signals are altered following heating to ~90 °C. (B) Effects of high temperature (98 °C) on the ice nucleation activity of *F. acuminatum*. Shown is the cumulative number of INs (N_m) per gram of mycelium plotted against the temperature. Data were obtained from Kunert *et al. (10).*

To obtain the distribution of heterogeneous ice nucleation temperatures of *F. acuminatum* INs, we extracted the differential freezing spectrum $n_m(T)$ from the experimental cumulative freezing spectrum $N_m(T)$ using the Heterogeneous Underlying-Based (HUB) backward numerical code (31). The code implements a stochastic optimization procedure that enables the fitting of the experimental $N_m(T)$ data, as shown in Fig. 3A, assuming a Gaussian distribution of nucleation temperatures in the sample. HUB-backward yields a differential spectrum $n_m(T)$ represented by a single population centered at −5.8°C (Fig. 3B). To interpret the position of the peak in the differential spectrum $n_m(T)$ of *F. acuminatum*, we use an accurate implementation of classical nucleation theory to predict ice nucleation temperatures of finite-sized IN surfaces (25). The calculation is implemented into a code known as the "Heterogeneous Ice Nucleation Temperature" (HINT), which takes into account the size and shape of the surface, and temperature-dependent thermodynamic and dynamic water properties to predict the temperature of heterogeneous ice nucleation (25). We assume that the ice-binding area of the fungal IN is a flat square surface with a binding energy $\Delta\gamma$ corresponding to that of ice-binding to ice. The predicted freezing temperatures based on a square surface are shown in Fig. 3C. We determine that the ice nucleation signal in the differential spectrum $n_m(T)$ of *F. acuminatum* corresponds to an ice-nucleating surface of ~250 nm^2, *i.e.* about 16 nm x 16 nm. Since we

assume maximum strength of $\Delta\gamma$, this estimate should be considered a lower limit to the size of the surface of the ice nucleating particles produced by *F. acuminatum.*

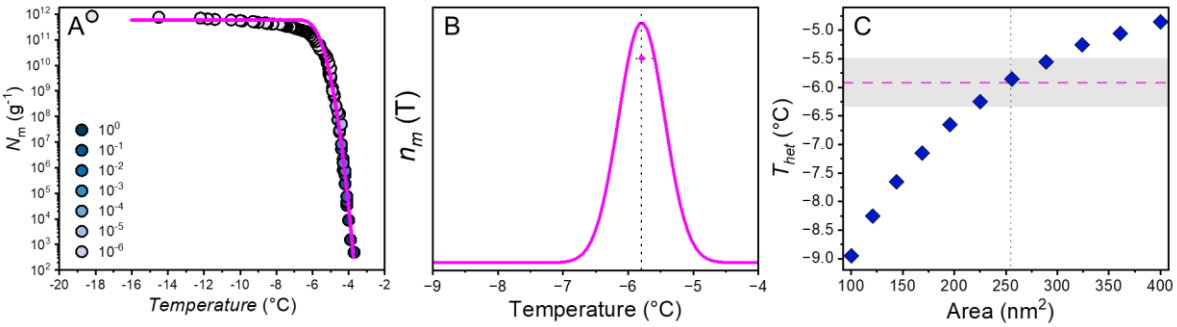

Fig. 3. Freezing experiments of aqueous extracts containing fungal INs from *F. acuminatum*. (A) Cumulative number of INs per unit mass of *F. acuminatum* (N_m) for extracts containing INs from spores and mycelial surfaces. The magenta line represents the optimized solution obtained through the HUB-backward code. (B) Normalized distribution function that represents the differential freezing spectrum $n_m(T)$ which gives the cumulative number of INs per unit mass. The magenta circle represents the temperature (−5.8 °C) which gives the mode of the distribution, and the black dotted lines represent the full-width-at-half-maximum. (C) Ice nucleation temperatures as a function of ice-binding area for the INs from *F. acuminatum.* Blue data points show the freezing temperatures on a square surface predicted by nucleation theory and the HINT algorithm. The mode (−5.8 °C) and the full-width at half-maximum of the underlying distribution of the heterogeneous freezing temperature are represented by the magenta line and the grey area, respectively.

Our theoretical estimate of the size of the IN surface responsible for the exceptional nucleation activity of *F. acuminatum* is consistent with the results of filtration experiments that showed N_m to be unchanged by filters with nominal cutoff down to 100 nm, minimally impacted by filters with nominal cutoff at ~9 nm (300 kDa), and strongly impacted by filters with smaller pores (Fig. S1) (10, 21). However, neither the filtration experiments nor our theoretical calculations can reveal whether the INs are composed of smaller subunits or their actual size. To address these questions, we used size exclusion chromatography (SEC), gel electrophoresis, and matrix-assisted laser desorption/ionization-time-of-flight (MALDI-TOF) spectroscopy of the purified *Fusarium* INs. Fig. 4A shows the SEC separation profile of standard calibration proteins and *Fusarium* INs in 50 mM sodium phosphate in 0.3 M NaCl buffer (pH 7.0). The elution profile of the *Fusarium* samples showed prominent peaks at ~5.20, ~7.40, ~10.98 and ~12.40 min (Fig. 4C). Based on the elution profile of the calibration proteins, we estimate the molecular weight of the *Fusarium* elution peaks to be ~660, ~45, ~12 and ~6 kDa, respectively.

Given that proteins can vary significantly in shape, the determined molecular weights of the *Fusarium* INs should not be seen as absolutes, but rather as good approximations. Interestingly, we find that smaller *Fusarium* fractions (even the ~12 kDa one) retained high ice nucleation activity (Fig. S2), supporting the hypothesis that *Fusarium* INs must consist of smaller subunits able to (re)assemble into larger IN.

The presence of small subunits with an estimated weight below 10 kDa is supported by MALDI spectra of ice-purified solutions of *F. acuminatum* and SDS-PAGE gel electrophoresis (Fig. 4B). A signal at ~5.3 kDa dominates the MALDI spectra, considering the 110 Da average molecular weight of amino acids, we estimate that this small protein unit contains ~48 amino acids. The SDS-PAGE gel shows a band at ~10 kDa, confirming the presence of small proteins. A globular protein of ~10 kDa would have a molecular diameter of ~1.4 nm, which is well below the minimal diameter of ~16 nm of a nucleation site required to initiate ice formation at -5.8 ˚C, according to our calculations using classical nucleation theory. Hence, we conclude that the *Fusarium* INs consist of small protein units that assemble into larger complexes in solution.

We assessed the minimum number of protein units needed to achieve the -5.8 ^{o}C peak nucleation temperature of *F. acuminatum* through a combination of experiments, nucleation theory, and modeling results. We estimated the ice nucleating area of the 5.3 kDa (~48 amino acids) protein assuming it has the structure and dimensions of the β-helix of the INP from *P. syringae* as predicted by AlphaFold2 (32). This results in an estimated 3.5 nm x 1.5 nm area per unit (see Supporting Information for details), and a minimum of ~50 units per aggregate. The mass of such an aggregate would be ~265 kDa. If we consider that only the 38% β-sheet sequence of the protein contributes to the nucleation site, the IN assembly would have ~130 units and a molecular weight of 697 kDa. This is in excellent agreement with the largest component detected in the size exclusion chromatography of the ice-purified solutions (Fig. 4A).

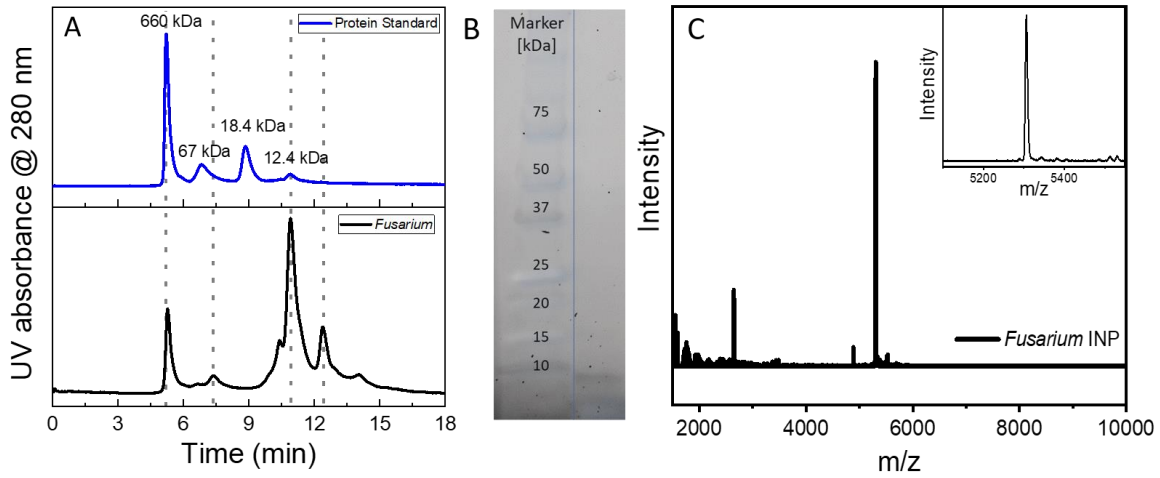

Fig. 4. Characterization of aqueous solutions of ice-purified INs from *F. acuminatum*. (A) Separation of a protein standard and *Fusarium* INs on a gel filtration column in 50 mM sodium phosphate in 0.3 M NaCl buffer (pH 7.0) at a flow rate of 1 mL/min. (B) SDS-PAGE gel electrophoresis shows a weak band <~10 kDa (C) MALDI spectra show a dominant signal at ~5300 which is highlighted in the inset.

Discussion:

Here we combine physicochemical characterizations of purified *Fusarium* INs with stochastic optimization algorithms and nucleation theory to unravel the nature and size of the units and functional assemblies that endow this fungus with outstanding ice nucleation ability. We find that the fungal INs consist of small protein subunits with about 50 amino acids, that assemble in aggregates containing over a hundred proteins in a cell-free environment to enable ice nucleation at high subzero temperatures. Similarly, small protein subunits released by the fungus *Mortierella alpina* also displayed ice-nucleating abilities (Fig. S2), suggesting that fungi display a common strategy of developing large IN from small protein units: *E pluribus unum*, out of many, one.

Our results support that the *E pluribus unum* strategy is consistently used by nature to produce the most efficient biological INs through the functional aggregation of smaller, weakly nucleating units. *P. syringae,* for instance, display INP aggregates in their outer membrane that can nucleate ice at high onset temperatures. However, individual bacterial INPs nucleate ice at just −25 °C, and the intact membrane is required to ensure functional aggregation (33, 34). Likewise, control of ice nucleation by assembling large units is also common in insects and

pollen, where a combination of carbohydrates, lipids, and proteins enables freezing (35, 36). Nature has implemented these *E pluribus unum* strategies using a wide range of sizes of building blocks –from <10 kDa proteins in fungi to ~120 kDa elongated proteins in bacteria– as well as environments for the functional assembly that encompass from extracellular soluble aggregates in fungi to membrane-bound assemblies in bacteria. In all cases, however, the functional assembly of smaller units results in a sufficiently large ice-binding area that can support the formation of the critical nucleus at temperatures above −5 °C. We expect that the energetic benefit for the organism in producing smaller, multifunctional proteins rather than a single large one, contributes to the success and widespread adoption of the *E pluribus unum* strategy across species that are not evolutionary related. We expect that the same strategies can be applied to design and produce synthetic INs by self-assembly of small ice-binding structures. Developing such powerful synthetic INs would be highly valuable for applications ranging from cryopreservation of cells to cloud seeding.

Methods:

Fungal culture and sample preparation. 75 plates of the ice nucleation-active fungal strain *Fusarium acuminatum* were grown on full-strength potato dextrose agar plates (VWR International GmbH, Darmstadt, Germany). Growth occurred at room temperature for one week and then at 6 °C for about four weeks. Pure water was obtained from Millipore Milli-Q® Integral 3 water purification system (Merck Chemicals GmbH, Darmstadt, Germany), autoclaved at 121 °C for 15 min, and filtered through a 0.1 µm bottle top filtration unit (VWR International GmbH, Darmstadt, Germany). For the droplet freezing experiments, aqueous extracts of fungal mycelium were prepared as described previously with the following modifications (10). The fungal mycelium of five agar plates was collected in a sterile 50 mL tube, and the weight of the mycelium was determined gravimetrically. Aliquots of 50 mL of pure water were added to the mycelium. The samples were vortexed three times at 2700 rpm for 1 min. The aqueous extracts for all experiments were filtered through a 0.1 µm bottle-top filtration unit (VWR International GmbH), and the resulting aqueous extracts contained ice nucleators from spores and mycelial surfaces. For filtration experiments, the 0.1 µm filtrate was filtered through either 30 kDa or 50 kDa MWCO PES ultrafiltration centrifugation units (Thermo Fisher Scientific, Braunschweig, Germany), and the ice nucleator concentration was determined by TINA measurements.

Ice affinity purification. Rotary ice-shell and ice-slide purification was used to purify the ice-nucleating macromolecules of the crude fungal extract. Details of the purification method have been described elsewhere(26, 27). In short, in a 500 mL flask, ~20–30 mL water was used to form an ice-shell using a dry ice-ethanol bath for 30–60 s. The flask was then rotated in a temperature-controlled ethylene glycol bath, and the temperature of the bath was set to −2 °C. 100 mL precooled fungal extract was added, and the flask rotated continuously in the bath until 30% of the solution was frozen. The ice was melted and freeze-dried to obtain a mixture of the ice-binding macromolecules present in *F. acuminatum*. The success of the purification was checked by determining the ice nucleation activity of the purified *Fusarium* samples using TINA measurements. The ice-purified solution was used for SEC experiments and to obtain MALDI, SDS-PAGE and CD spectra.

Size exclusion chromatography.

The crude ice-purified extract was lyophilized and dissolved in water. The protein in the clear solution (~4 mg/mL) was analyzed by HPLC using a G2000SWXL TSK gel column (7.6 mm x 30 cm). The elution buffer was 0.05 M sodium phosphate in 0.3 M NaCl, pH 7.0. The flow rate was 1 mL/min, with absorbance recorded at 220 nm.

SDS-PAGE

Protein samples were mixed with a fifth volume of 6x Laemmli buffer containing 5% of β-Mercaptoethanol and were heated at 95 °C for 5 min. Samples were loaded onto a MiniPROTEAN® TGX™ Stain-free Precast Protein Gel (4-20%, Bio-Rad, Munich, Germany) next to a molecular weight marker (Precision Plus Protein Unstained Standards, 161-0363, Bio-Rad). The electrophoresis setting was a constant voltage of 175 V for 40 min. Image acquisition of the gel was performed using a ChemiDoc MP Imaging system and the Image Lab software (Version 5.1, Bio-Rad).

TINA experiments. Ice nucleation experiments were performed using the high-throughput Twin-plate Ice Nucleation Assay (TINA), which has been described in detail elsewhere (23). In a typical experiment, the investigated IN sample was serially diluted 10-fold by a liquid handling station (epMotion ep5073, Eppendorf, Hamburg, Germany). 96 droplets (3 µL) per dilution were placed on two 384-well plates and tested with a continuous cooling rate of 1 °C/min from 0 °C to −20 °C with a temperature uncertainty of ±0.2 °C. The droplet-freezing was determined by two infrared cameras (Seek Therman Compact XR, Seek Thermal Inc., Santa Barbara, CA, USA). The obtained fraction of frozen droplets was used to calculate the cumulative number of ice nucleators using the Vali formula (24). All experiments were performed multiple times (e.g., Fig. 1, 3-5 samples) with independent samples. Background freezing of pure (autoclaved MilliQ) water in our system occurred at ~−25 °C.

CD spectroscopy. CD spectra were recorded at a 1 nm interval from 260 to 180 nm using a Jasco J-1500 spectrometer. CD measurements were performed in a rectangular cell with the optical path of 0.1 cm. Equilibration time for every sample before each set of measurements was 15 min. All spectra were background subtracted and processed using the Spectra Manager Analysis program from JASCO.

MALDI-TOF. MALDI measurements were carried out on a rapifleXTM MALDI-TOF/TOF mass spectrometer from Bruker Daltonik GmbH. The instrument is equipped with a scanning smartbeam 3D 10 kHz Nd:YAG laser at a wavelength of 355 nm and a 10-bit 5 GHz digitizer. The acceleration voltage was set to 20 kV and the mass spectra were recorded in positive ion mode. Calibration was done with the Bruker peptide mix and the Bruker protein calibration standard I and II in a mass range of up to 70 kDa. Sample preparation was done by mixing a saturated solution of sinapinic acid dissolved in water/acetonitrile (1:1 + 0,1 % trifluoroacetic acid) with an aqueous solution of the analyte in equal amounts. Samples were measured with random walk ionization across the sample spot. Typically, 8000 shots were averaged per spectrum.

Nanoliter Cryoscopy. Ice shaping was determined at a *Fusarium* concentration of ~10 mg/mL in water using a Clifton Nanoliter Osmometer (37). Ice shaping was performed with a cooling rate of 0.075 °C/min and without annealing. Measurements were performed 2-4 times on independent samples.

HUB method. We used the HUB-backward stochastic optimization code to extract the distribution of heterogeneous ice nucleation temperatures from the experimental cumulative

nucleation spectra (31). The HUB code uses the same assumptions adopted by Vali (24). It considers that the number of IN in each droplet follows the Poisson distribution, that each IN has a distinct nucleation temperature, and that the IN with the warmest nucleation temperature in the droplet sets the freezing temperature of the droplet in the cooling experiment. The HUB-backward code represents the distribution of nucleation temperatures of the IN in the sample as a linear combination of Gaussian populations and uses a stochastic optimization procedure to find the best set of parameters of the populations: modes, widths and weights to reproduce the experimental $N_m(T)$. The output of the HUB-backward is the differential spectrum $n_m(T)$ in terms of the distribution of subpopulations of INs that reproduce the cumulative freezing spectrum $N_m(T)$ of *Fusarium*. We find that a single subpopulation represents well the experimental data for the fungus.

Classical Nucleation Theory (CNT). The HINT algorithm is an accurate numerical implementation of classical nucleation theory that predicts the temperatures of heterogeneous nucleation of ice on finite-sized IN surface using experimental data for water such as the self-diffusion coefficient D, the difference in chemical potential between liquid and ice $\Delta\mu$, and the ice-liquid surface tension $\gamma_{ice\text{-}liquid}$, the surface binding free energy of the IN to ice $\Delta\gamma_{bind} = \gamma_{ice\text{-}IN} - \gamma_{ice\text{-}liquid} - \gamma_{liquid\text{-}IN}$, where $\gamma_{ice\text{-}IN}$ and $\gamma_{liquid\text{-}IN}$ are the surface tensions of the ice nucleating surface with ice and liquid water, respectively (25). HINT uses that data to compute the free energy barriers for ice nucleation and the prefactor for the nucleation rate. It predicts the nucleation temperature with that data and knowledge of the experimental nucleation rate $J_{exp} = 10^5$ cm^{-3} s^{-1} corresponding to cooling microliter at rates of 1 Kmin^{-1} (38-40). For simplicity, we assume the IN surface is a square, and that the IN binds ice as strong as ice itself, i.e. $\Delta\gamma_{bind} = -2\,\gamma_{ice\text{-}liquid}$. The latter approximation implies that our estimate of the surface of the fungal IN is a lower bound of its actual value.

Corresponding Author

Konrad Meister, e-mail: meisterk@mpip-mainz.mpg.de

Valeria Molinero, e-mail: valeria.molinero@utah.edu

Notes

The authors declare no competing financial interests.

Acknowledgment

We are grateful to the MaxWater initiative from the Max Planck Society and the Deutsche Forschungs Gemeinschaft (ME 5344/1-1). K. M. acknowledges support by the National Science Foundation under Grant No. (NSF 2116528) and from the Institutional Development Awards (IDeA) from the National Institute of General Medical Sciences of the National Institutes of Health under Grants #P20GM103408, P20GM109095. I. de A. R. and V. M. gratefully acknowledge support by AFOSR through MURI Award No. FA9550-20-1-0351. We thank N.-M. Kropf and L. Reichelt for technical assistance and the Center for High Performance Computing at the University of Utah for an award of computing time and technical support.

References

1. H. Laksmono *et al.*, Anomalous Behavior of the Homogeneous Ice Nucleation Rate in "No-Man's Land". *The Journal of Physical Chemistry Letters* **6**, 2826-2832 (2015).
2. B. J. Murray, D. O'Sullivan, J. D. Atkinson, M. E. Webb, Ice nucleation by particles immersed in supercooled cloud droplets. *Chemical Society Reviews* **41**, 6519-6554 (2012).
3. D. Gurian-Sherman, S. E. Lindow, Bacterial ice nucleation: significance and molecular basis. *Faseb j* **7**, 1338-1343 (1993).
4. A. G. Govindarajan, S. E. Lindow, Size of Bacterial Ice-Nucleation Sites Measured in Situ by Radiation Inactivation Analysis. *Proc. Natl. Acad. Sci. U.S.A.* **85**, 1334 (1988).
5. S. E. Lindow, E. Lahue, A. G. Govindarajan, N. J. Panopoulos, D. Gies, Localization of ice nucleation activity and the iceC gene product in Pseudomonas syringae and Escherichia coli. *Mol Plant Microbe Interact* **2**, 262-272 (1989).
6. G. M. Mueller, P. K. Wolber, G. J. Warren, Clustering of ice nucleation protein correlates with ice nucleation activity. *Cryobiology* **27**, 416-422 (1990).
7. P. K. Wolber *et al.*, Identification and purification of a bacterial ice-nucleation protein. *Proceedings of the National Academy of Sciences* **83**, 7256-7260 (1986).
8. C. Orser, B. J. Staskawicz, N. J. Panopoulos, D. Dahlbeck, S. E. Lindow, Cloning and Expression of Bacterial Ice Nucleation Genes in Escherichia Coli. *J. Bacteriol.* **164**, 359 (1985).
9. S. Pouleur, C. Richard, J. G. Martin, H. Antoun, Ice Nucleation Activity in Fusarium acuminatum and Fusarium avenaceum. *Appl Environ Microbiol* **58**, 2960-2964 (1992).
10. A. T. Kunert *et al.*, Macromolecular fungal ice nuclei in Fusarium: effects of physical and chemical processing. *Biogeosciences* **16**, 4647-4659 (2019).
11. J. Fröhlich-Nowoisky *et al.*, Ice nucleation activity in the widespread soil fungus Mortierella alpina. *Biogeosciences* **12**, 1057-1071 (2015).
12. J. A. Huffman *et al.*, High concentrations of biological aerosol particles and ice nuclei during and after rain. *Atmos. Chem. Phys.* **13**, 6151-6164 (2013).
13. C. E. Morris *et al.*, Urediospores of rust fungi are ice nucleation active at > −10 °C and harbor ice nucleation active bacteria. *Atmos. Chem. Phys.* **13**, 4223-4233 (2013).
14. V. Després *et al.*, Primary biological aerosol particles in the atmosphere: a review. *Tellus B: Chemical and Physical Meteorology* **64**, 15598 (2012).
15. R. Du *et al.*, Evidence for a missing source of efficient ice nuclei. *Scientific Reports* **7**, 39673 (2017).
16. C. M. Beall *et al.*, Cultivable halotolerant ice-nucleating bacteria and fungi in coastal precipitation. *Atmos. Chem. Phys.* **21**, 9031-9045 (2021).
17. M. N. Smith, Pathological Factors Affecting Survival of Winter Barley Following Controlled Freeze Tests. *Phytopathology* **68**, 773 (1978).

18. D. O'Sullivan *et al.*, The relevance of nanoscale biological fragments for ice nucleation in clouds. *Scientific Reports* **5**, 8082 (2015).
19. Y. Hasegawa, Y. Ishihara, T. Tokuyama, Characteristics of ice-nucleation activity in Fusarium avenaceum IFO 7158. *Biosci Biotechnol Biochem* **58**, 2273-2274 (1994).
20. Y. Hasegawa, Y. Ishihara, T. Tokuyama, Characteristics of Ice-Nucleation Activity in Fusarium Avenaceum Ifo 7158. *Biosci., Biotechnol., Biochem.* **58**, 2273 (1994).
21. S. Yang, M. Rojas, J. J. Coleman, B. A. Vinatzer, Identification of Candidate Ice Nucleation Activity (INA) Genes in Fusarium avenaceum by Combining Phenotypic Characterization with Comparative Genomics and Transcriptomics. *Journal of Fungi* **8**, 958 (2022).
22. P. E. Nelson, M. C. Dignani, E. J. Anaissie, Taxonomy, biology, and clinical aspects of Fusarium species. *Clinical Microbiology Reviews* **7**, 479-504 (1994).
23. A. T. Kunert *et al.*, Twin-Plate Ice Nucleation Assay (Tina) with Infrared Detection for High-Throughput Droplet Freezing Experiments with Biological Ice Nuclei in Laboratory and Field Samples. *Atmos. Meas. Technol.* **11**, 6327 (2018).
24. G. Vali, Quantitative Evaluation of Experimental Results an the Heterogeneous Freezing Nucleation of Supercooled Liquids. *Int. J. Atmos. Sci.* **28**, 402 (1971).
25. Y. Qiu, A. Hudait, V. Molinero, How Size and Aggregation of Ice-Binding Proteins Control Their Ice Nucleation Efficiency. *Journal of the American Chemical Society* **141**, 7439-7452 (2019).
26. H. E. Tomalty, L. A. Graham, R. Eves, A. K. Gruneberg, P. L. Davies, Laboratory-Scale Isolation of Insect Antifreeze Protein for Cryobiology. *Biomolecules* **9**, 180 (2019).
27. M. Lukas *et al.*, Interfacial Water Ordering Is Insufficient to Explain Ice-Nucleating Protein Activity. *The Journal of Physical Chemistry Letters* **12**, 218-223 (2021).
28. A. Micsonai *et al.*, Accurate secondary structure prediction and fold recognition for circular dichroism spectroscopy. *Proceedings of the National Academy of Sciences* **112**, E3095-E3103 (2015).
29. X. Wang *et al.*, A mutant of hydrophobin HGFI tuning the self-assembly behaviour and biosurfactant activity. *Applied Microbiology and Biotechnology* **101**, 8419-8430 (2017).
30. C. P. Garnham, R. L. Campbell, V. K. Walker, P. L. Davies, Novel dimeric β-helical model of an ice nucleation protein with bridged active sites. *BMC Struct Biol* **11**, 36 (2011).
31. I. de Almeida Ribeiro, K. Meister, V. Molinero, HUB: A method to model and extract the distribution of ice nucleation temperatures from drop-freezing experiments. (2022).
32. H.-B. Guo *et al.*, AlphaFold2 models indicate that protein sequence determines both structure and dynamics. *Scientific Reports* **12**, 10696 (2022).
33. Y. Qiu, A. Hudait, V. Molinero, How Size and Aggregation of Ice-Binding Proteins Control Their Ice Nucleation Efficiency. *J. Am. Chem. Soc.* **141**, 7439 (2019).
34. R. Schwidetzky *et al.*, Membranes Are Decisive for Maximum Freezing Efficiency of Bacterial Ice Nucleators. *J. Phys. Chem. Lett.* **12**, 10783 (2021).
35. K. L. Yeung, E. E. Wolf, J. G. Duman, A scanning tunneling microscopy study of an insect lipoprotein ice nucleator. *Journal of Vacuum Science & Technology B: Microelectronics and Nanometer Structures Processing, Measurement, and Phenomena* **9**, 1197-1201 (1991).
36. K. Dreischmeier, C. Budke, L. Wiehemeier, T. Kottke, T. Koop, Boreal pollen contain ice-nucleating as well as ice-binding 'antifreeze' polysaccharides. *Scientific Reports* **7**, 41890 (2017).
37. Y. Sun *et al.*, Disaccharide Residues are Required for Native Antifreeze Glycoprotein Activity. *Biomacromolecules* **22**, 2595-2603 (2021).
38. T. Koop, B. Luo, A. Tsias, T. Peter, Water activity as the determinant for homogeneous ice nucleation in aqueous solutions. *Nature* **406**, 611-614 (2000).
39. T. Koop, B. J. Murray, A physically constrained classical description of the homogeneous nucleation of ice in water. *The Journal of Chemical Physics* **145**, 211915 (2016).
40. L. Kaufmann, C. Marcolli, B. Luo, T. Peter, Refreeze experiments with water droplets containing different types of ice nuclei interpreted by classical nucleation theory. *Atmos. Chem. Phys.* **17**, 3525-3552 (2017).

455